Solid Freeform Fabrication 2023: Proceedings of the 34th Annual International Solid Freeform Fabrication Symposium – An Additive Manufacturing Conference
Reviewed Paper

MODELING CARBON FIBER SUSPENSION DYNAMICS FOR ADDITIVE MANUFACTURING POLYMER MELT FLOWS

Jason B. Pierce*, Douglas E. Smith*

*Department of Mechanical Engineering, Baylor University, Waco, TX 76798

*Corresponding Author Email: Jason_Pierce1@Baylor.edu

Abstract

The addition of short carbon fibers to the feedstock of large-scale polymer extrusion/deposition additive manufacturing results in significant increases in mechanical properties dependent on the fiber distribution and orientation in the beads. In order to analyze those factors, a coupled computational fluid dynamics (CFD) and discrete element modeling (DEM) approach is developed to simulate the behavior of fibers in an extrusion/deposition nozzle flow after calibrations in simple shear flows. The DEM model uses bonded discrete particles to make up flexible and breakable fibers that are first calibrated to match Jeffery's orbit and to produce interactions that are consistent with Advani-Tucker orientation tensor predictions. The DEM/CFD model is then used to simulate the processing of fiber suspensions in the variable flow and geometries present in extrusion/deposition nozzles. The computed results provide enhanced insight into the evolution of fiber orientation and distribution during extrusion/deposition as compared to existing models through individual fiber tracking over time and space on multiple parameters of interest such as orientation, flexure, and contact forces.

Introduction

Polymer extrusion/deposition additive manufacturing is a rapidly growing area of research in industry and academia with particular focus on how to optimize the process and control microstructure. In fused filament fabrication (FFF), a wide variety of polymers are available for both large area and small-scale printers. Carbon fibers are often added to the polymer feedstock which affects both mechanical and thermal properties of the composite during processing while creating final parts that are structurally superior as compared to those produced with neat polymers. These fibers improve mechanical properties such as the modulus of elasticity and tensile strength while increasing thermal conductivity and decreasing the coefficient of thermal expansion. The degree of improvement achieved through the addition of carbon fibers is highly dependent on the orientation of the fibers relative to the applied loads [1]. This fiber orientation is affected by printing parameters such as extrusion rate, print speed, nozzle geometry, fiber characteristics, and layer height [2]. In order to optimize part strength, the mechanisms of fiber orientation changes over time and space in complex flows and the factors that impact them must be well understood.

Significant advances have been seen in the field of simulating fiber orientation evolution. The motion of a single isolated rigid ellipsoidal fiber in simple shear, often referred to as Jeffery's Orbit, is the first step in modeling fiber motion [3]. This work was expanded to include fiber-fiber interaction with the commonly used tensor description of fiber suspension orientation states by Advani and Tucker [4]. Phan-Thien proposed equations to predict the Advani-Tucker interaction coefficient C_i for isotropic diffusion based on the fiber volume fraction and aspect ratio [5]. The Advani-Tucker equations and other prediction models [6] have been applied to streamlines from

finite element-based flow simulations of additive manufacturing nozzle flows [7,8] while other single fiber motion studies have yielded a better understanding of the mechanics of fiber suspensions in flow processes [9–11].

Fiber motion and interaction has been the primary focus of short fiber polymer composite flow modeling which has been limited to rigid fibers where little attention has been given to including fiber breakage in the models [9,12,13]. Modeling individual fiber breakage and flexure is essential for accurate simulation of FFF nozzles as fibers are shorter in the prints than the feedstock for both the short fibers used in small scale printing [1] and the long fibers that interact with the screw-generated flows in large scale printing [14].

Many existing models are limited by some of their core assumptions. For example, models derived from Jeffery's original work assume that fibers are rigid and ellipsoidal [3]. Neither the flow nor the fibers have mass, and therefore do not experience the effects of inertia. The fiber interaction models assume a homogeneous fiber distribution and are based on phenomenological constants that attempt to capture random rotary diffusion rather than directly having fibers interact with each other and result in a statistical model of orientation state [4]. Fibers are assumed to be far from boundary conditions, which makes applications with potential for wall effects difficult to simulate. The assumptions were essential to simplify calculations for the available computational power of the time but deviate from realism and fail to capture the complete fiber state.

Discrete element modeling (DEM) is a simulation technique that models the interactions of particles in granular materials [15]. The individual particles interact with each other and adjacent fixed geometries through contact models. These solid interactions can occur simultaneously with fluid interactions when DEM is coupled with computational fluid dynamics (CFD) [16]. Particles in DEM can be selectively connected together with beamlike bonds to create metaparticles that can be calibrated to flex and break or act like rigid solids [17]. The particles have mass and experience inertia. These capabilities enable the direct simulation of fibers while providing avenues to address the assumptions that limit Jeffery-based models. With current advances in computational power, DEM enables the simulation of a high number of particles that interact with the flow, surrounding fixed geometry, and each other. Similar advances in the ability to experimentally measure fiber orientation and other relevant factors in 3D provide the possibility for the simulations to be validated [18]. With a well calibrated and validated DEM model, new analysis of fiber motion becomes possible.

This paper uses DEM to simulate the flow and interaction of a collection of fibers typical of small scale polymer composite extrusion/deposition additive manufacturing. Calibration of the DEM model begins with the motion of a single rigid fiber in flows with known analytical solutions for the orientation evolution. With appropriate single fiber motion, fiber-fiber interactions are then tuned to achieve the expected fiber suspension behavior. Fibers that behave appropriately in flows can then have realistic stiffnesses and strengths applied enabling more realistic simulations with fewer assumptions. Properly calibrated DEM fiber suspensions are then used to provide enhanced insights into the mechanisms of fiber motion during FFF printing. These DEM models can then be used to enable process optimization and guide component design for both printers and final parts.

Methodology

Discrete Element Method – Simulation Setup

Discrete Element Method simulations are based on a few key physics which determine how the particles that make up the carbon fibers interact with the flow, each other within a fiber, each other between fibers, and the surrounding fixed geometry. Drag models are employed to control fiber-flow interaction behavior while bonding parameters influence the intra-fiber particle-particle physics. Fibers interact with each other and the wall geometry through contact models with friction, restitution, and damping. In order to achieve realistic behavior in the final nozzle simulations these interactions need to be properly calibrated through parameter selection. This study uses EDEM Simulations (Altair Engineering, Troy, Michigan, USA) as the DEM solver.

Drag models are used in DEM simulations to control how the individual particles that make up the fibers are moved by the flow. The DEM solver references flows through uni-directional or bi-directional coupling with CFD. In uni-directionally coupled simulations, the flow field is pre-established without out any consideration for the fibers other than effective changes to properties such as the viscosity and is most appropriate for cases where the DEM simulated component is considered to have minimal contribution to the fluid flow solution. Within the DEM solver, values of fluid velocity in the flow field are obtained from the completed CFD solution and imported as a fixed vector field. In bi-directional coupling, the CFD and DEM are coupled such that the flow velocities, pressures, and particle shape and locations are computed together in an iterative manner. Solutions obtained with bi-directional coupling are more computationally expensive, but can capture the influence of particles on the flow. A variety of options are typically available in commercially available DEM solvers such as Altair's EDEM Simulations. For example, the Schiller and Naumann drag model is commonly used for the spherical particles which used to model single fibers here. The Schiller and Newmann model, shown in Eqn. 1 [19], needs user inputs for the Reynolds Number Re which is used to determine the drag coefficient C_D. The resultant drag force f_{Drag} acts through the center of particles providing a translational force in the direction of the flow relative to the motion of the fiber.

$$f_{Drag} = \frac{C_D Re}{24} \quad where \quad C_D = \begin{cases} 24\left(1 + 0.15\mathrm{Re}^{0.687}\right) / \mathrm{Re} & Re \leq 1000 \\ 0.44 & Re > 1000 \end{cases} \tag{1}$$

In our short fiber polymer composites models, a sufficiently high viscosity combined with the low density of carbon fibers essentially eliminates the inertia of fibers as the drag model forces the particles to follow the flow. This negligible inertia case is used during initial calibration to align with the assumptions used in the models that the DEM results will be compared against.

Particles are held together in meta-particles with pre-arranged layouts that are held together with beam-like bonds to form slender rod-like fibers in our simulations. These bonds transfer forces as well as torques between particles to simulate intra-fiber stiffness and strengths. The bonds result in flexible meta-particles with established shear and normal stiffnesses that can break if the ultimate strength is exceeded. The forces in the bonds are calculated each iteration and require an appropriate timestep to avoid unrealistically high forces. When the bonds break, they will not be reformed, but the particles can come into contact again. In this study, sufficiently high bond strengths and stiffnesses are assumed to avoid fiber bending and breakage.

Particles interact with others they are not bonded to and the surrounding fixed geometry that bound the simulation domain through a Hertz-Mindlin contact model and a rolling friction model [17,20,21]. The no-slip Hertz-Mindlin model provides a damping force to slow and stop particles as they approach each other. These fiber-fiber interaction governing equations are

calibrated in this study by tuning the coefficients of friction and restitution during the fiber suspension simulations until the time-dependent orientation state matches that predicated by Advani-Tucker orientation tensor models [4]. In the work presented below, parameters in the Hertz-Mindlin contact model are adjusted to obtain results that agree with those computed using the Advani-Tucker models. The summation of forces and torques from the fluid, bonds, and contacts on particle determine its motion in DEM.

Post-simulation analysis is completed using custom Matlab scripts with important fiber orientation assessment parameters calculated from DEM output data. Information for each individual particle such as positions, velocities, current forces, and bond status is recorded for each saved timestep. Scripts are used to organize particle data by the meta-particle fibers they compose, making each particle analogous to a sensor placed on the fiber. The 3D orientation vector components p_i, i = 1,2,3 of these fibers can be obtained by calculating and normalizing the distance between two endpoints of a rigid fiber, resulting in a unit vector that describes the orientation of the fiber. These vectors can then be orientation-averaged to provide results over a collection of fibers. The DEM simulations provide a rich environment to analyze the mechanisms of well calibrated fibers with a wide breadth of information available about each fiber. Fibers can be tracked through time and space and compared to their neighbors from Eulerian and Lagrangian perspectives for single fibers or fiber suspension behavior over regions.

Single Fiber Simulations

Calibration of the DEM fiber model begins with the behavior of a single isolated fiber in simple shear flow which is compared with Jeffery's orbit [3]. The fibers are bonded meta-particles forming an extruded hexagon as shown in Fig. 1. This layout is chosen to place the particle centroids off of the centerline of the fiber. This separation from the axis is essential to allow the fiber to continue rotating when aligned with the flow since the drag models in DEM solvers generally act through centroids and do not produce torques. The extruded hexagon balances the need for this offset and 3D axial symmetry with keeping the number of particles low enough for reasonable computation time. Other layouts can similarly achieve these goals and potentially incorporate multi-sphere or spherocylinder particles.

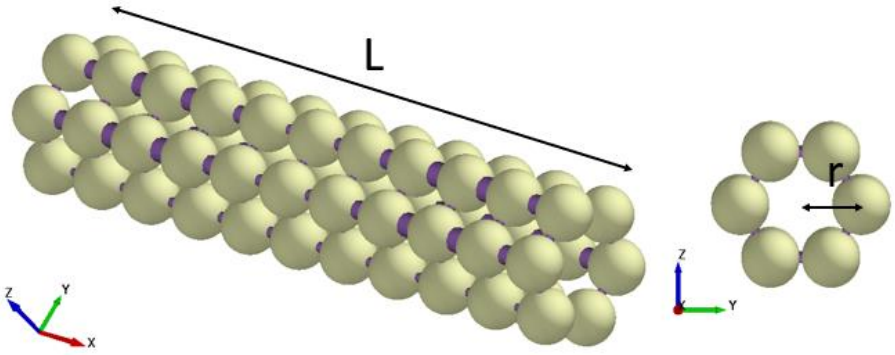

Fig. 1 - Extruded hexagon fiber layout with parameters of length L and effective radius r

The meta-particle fibers are calibrated in unidirectionally coupled simple shear flows with constant shear rates and periodic boundaries. Flow velocity vectors are computed from the empirical solution for simple shear flow with the flow rate increasing in the Z direction and constant in the X-Y plane as designated in Eqn. 2 where $|\dot{\gamma}|$ is the shear rate magnitude, and $v_X, v_Y,$

and v_Z are the X,Y,Z components of the fluid velocity at a given point in the domain with v_X as a function of Z position. These vectors are evenly spaced throughout the domain.

$$v_X(Z) = |\dot{\gamma}|Z$$
$$v_Y = v_Z = 0 \quad (2)$$

The period of the fiber can be tuned by slightly altering the location of the particles relative to the axis of the fiber. Once a fiber is simulated in flow, the layout can be iteratively change until the rotation matches Jeffery's orbit, obtained by solving for the components of the unit orientation vector, p_i, in Eqn. 3 for a given isolated bead aspect ratio [3,9]. The fiber aspect ratio is denoted as a_r. The fluid shear stress tensor components are $\dot{\gamma}_{ij}$ and the vorticity is ω_{ij}, with i,j=1,2,3. Alternatively, an optimization scheme may be used to iteratively find the aspect ratio that a given layout replicates.

$$\dot{p}_i = -\frac{1}{2}(\omega_{ij}p_j) + \frac{1}{2}\lambda(\dot{\gamma}_{ij}p_j - \dot{\gamma}_{kl}p_k p_l p_i) \; where \; \lambda = \frac{{a_r}^2 - 1}{{a_r}^2 + 1} \quad (3)$$

Fiber Interaction Simulations

With a properly calibrated fiber-flow behavior for a single fiber, the fiber-fiber interactions are adjusted to behave according to the Advani-Tucker equations. A schematic of the simulation domain is shown in Figure 2. The simulation domain is set up with periodic boundaries in X and Y to emulate an infinite plane. A periodic boundary in Z would cause fibers crossing the boundary to experience an extreme shear rate change between the slower flow at the -Z limit and fast flow at the +Z limit, so walls are used to prevent fibers from leaving the domain. In order to prevent potential wall affects, the analysis is completed sufficiently far from the walls. The flow is the same simple shear used in calibrating a single fiber.

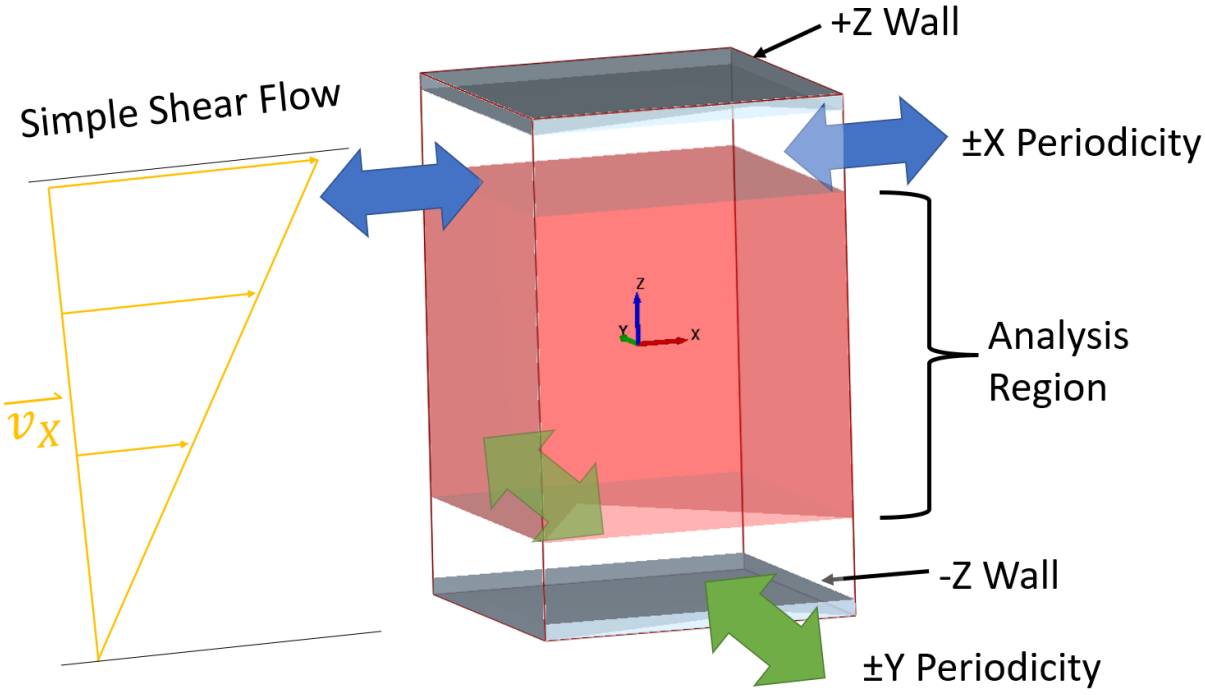

Fig. 2 – Simulation domain and flow field for bulk fiber simulations

Fibers are generated in the initial timestep with random positions and orientations. The number of fibers generated determines the fiber volume fraction in the fixed volume domain. The simulation proceeds with fibers interacting with each other and the flow until sufficient time has passed to reach a steady state. From there, the outer product of every individual fibers' orientation, described by p_i, is taken with itself and averaged for each timestep as shown in Eqn. 4 [4] with N as the number of fibers analyzed. $A_{ij,DEM}$ is the components of the tensor representation of the orientation state of a group of fibers in DEM at a given timestep and is directly comparable to the Advani-Tucker orientation tensor.

$$A_{ij,DEM} = \frac{1}{N}\sum_{1}^{N}(p_i p_j) \tag{4}$$

An optimization scheme shown in Equation 5 is used to minimize the absolute difference between the expected results from Advani-Tucker, $A_{ii,AT}$, and the average alignment from the DEM simulation, $A_{ii,DEM}$, at each timestep integrated over the total simulation time T. The equation is normalized by T to enable comparison between simulations run for differing time periods.

$$F = \frac{1}{T}\int_0^T \left(\left|A_{11,AT} - A_{11,DEM}\right| + \left|A_{22,AT} - A_{22,DEM}\right| + \left|A_{33,AT} - A_{33,DEM}\right|\right) \tag{5}$$

Equation 5 is one of many potential objective functions that can be used. The effective C_i is the value that minimizes F for a given DEM fiber suspension simulation. The $A_{ii,AT}$ values used in this comparison are the solutions from evaluating the Advani-Tucker equation, Eqn. 6 [4], with a fourth order Runge-Kutta and an orthotropic closure using the same initial conditions as in DEM. The closure is required to resolve the 4th order orientation tensor A_{ijkl}. Equation 6 uses δ_{ij} as the Kronecker delta function and λ is as defined in Equation 3.

$$\begin{aligned}\frac{DA_{ij}}{Dt} = &-\frac{1}{2}\left(\omega_{ik}A_{kj} - A_{ik}\omega_{kj}\right) + \frac{1}{2}\lambda\left(\dot{\gamma}_{ik}A_{kj} - A_{ik}\dot{\gamma}_{kj} - 2\dot{\gamma}_{kl}A_{ijkl}\right) \\ &+ 2\left(C_i|\dot{\gamma}|\right)\left(\delta_{ij} - 3A_{ij}\right)\end{aligned} \tag{6}$$

The effective C_i from the DEM simulations is tuned through the contact model's coefficients of friction and restitution. A design of experiments method can be used to find the proper combination of coefficients for a given volume fraction, ϕ, and aspect ratio, a_r, according to the Phan-Thien curve, Eqn. 7.

$$C_i = 0.03[1 - exp(-0.224a_r\phi)] \tag{7}$$

Nozzle Simulations

Well calibrated fiber suspension behavior of fibers lends confidence to proceed with simulations of fiber filled polymer flows typically used in small scale additive manufacturing nozzles. The process begins with generation of a 3D CAD model for the nozzle. For these preliminary nozzle simulations, a simple 1.85 mm to .4 mm converging nozzle is used, as shown in Figure 3. This geometry is then treated as walls for the CFD and DEM solvers. In CFD, a shaped velocity inlet is used with an atmospheric pressure outlet. The CFD simulation is run to steady state, then the velocity vectors are exported to the DEM solver for a unidirectionally coupled simulation.

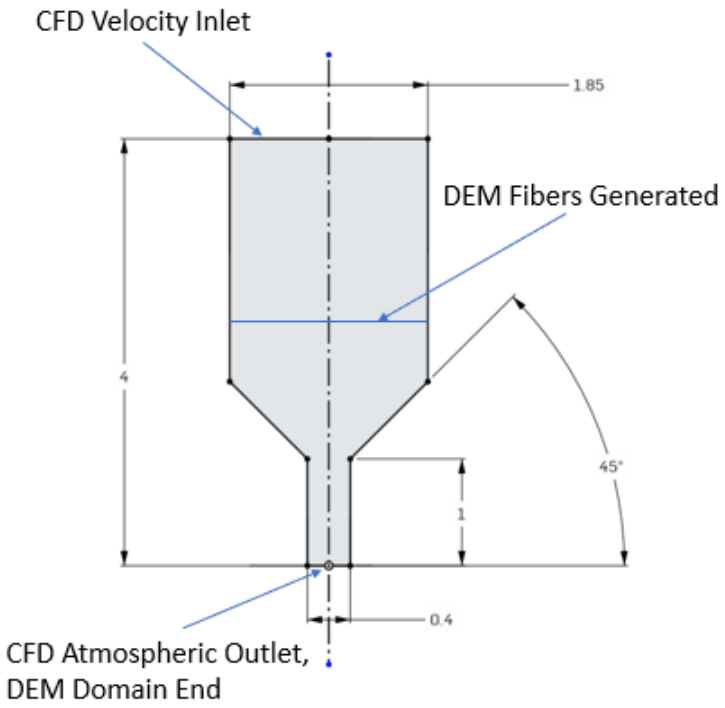

Fig. 3 - Cross section of 3D nozzle geometry with units in mm

The nozzle models are set up with the parameters determined during the single and fiber suspension calibrations. Fibers are generated with random position and orientation across the nozzle above the point of convergence and allowed to evolve in the flow. This method of fiber generation is analogous to placing fibers mid-stream in an already flowing nozzle. If desired, the positions and orientations can be pre-determined, such as starting with regularly spaced fully aligned fibers. The flow rate of polymer through the nozzle, nozzle geometry, and fiber parameters such as aspect ratio, stiffness, and volume fraction can be changed as independent inputs into the nozzle simulations.

Results and Discussion

Single Fiber – Jeffery's Orbit

Jeffery's orbit was consistently achieved for fibers of various aspect ratios under a variety of conditions. Fiber orientation at various values of simulation time appear in Fig. 4 along with a comparison of p_3 values from the DEM simulations and Jeffery's orbit. The graph shows significant alignment over several orbits for a 5.04 isolated bead hydrodynamic aspect ratio. The results shown in Fig. 5 shows the fiber orientation evolution for three shear rates aligning reasonably well with the expected Jeffery's orbit for a fiber initially calibrated at a shear rate (SR) of 10. The agreement in alignment for each of the shear rates demonstrates that the model is fairly robust even outside of its calibration point. This consistency is maintained well over several orbits. As long as the centroid location of the particles in the layout is maintained, differently sized and shaped particles behave similarly, allowing some difference between the physical aspect ratio of the fiber and the hydrodynamic aspect ratio. The viscosity and density of the fluid do not impact the orbit in alignment with Jeffery's equations. This behavior also holds in DEM so long as they are sufficient to overcome any inertial behavior of the fiber. Uniformly scaling fiber size similarly

maintains the orbit with constant aspect ratio. These behaviors are the expected result, as those flow and scale parameters are not included in traditional fiber orientation evolution models.

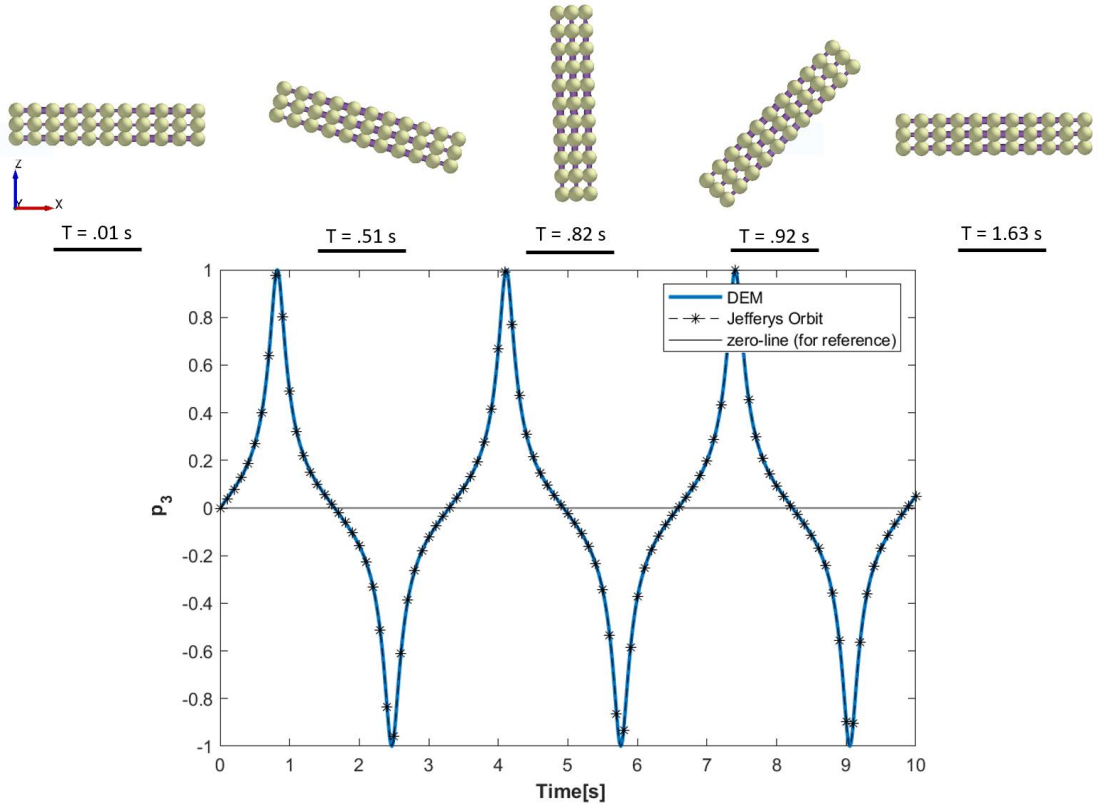

Fig. 4 - Isolated fiber orbits in simple shear flow with shear rate 10 and hydrodynamic aspect ratio 5.04 along with snapshot of the bonded metaparticle fibers at given times

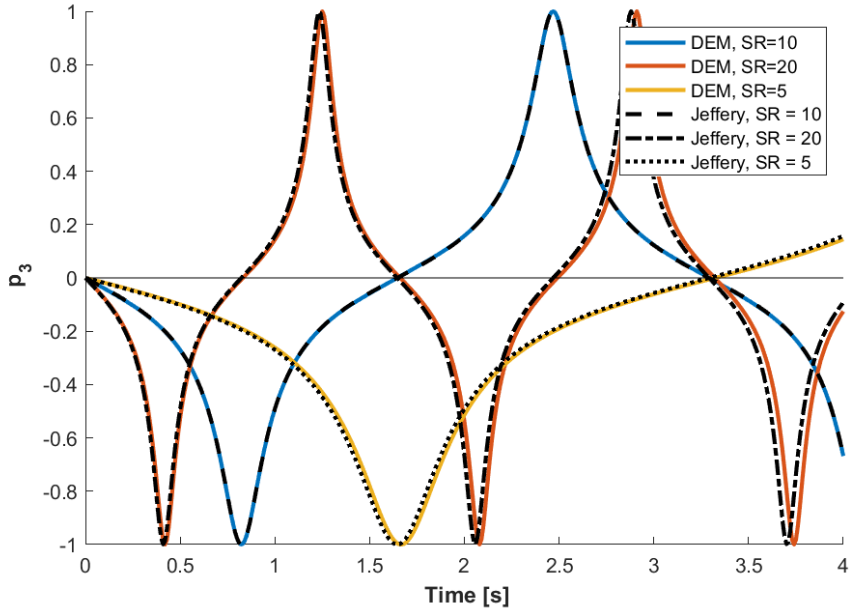

Fig. 5 – p_3 component of the single fiber's orientation compared to Jeffery's Orbit for shear rates (SR) of 5, 10, and 20

Fiber Suspension Simulations – Coefficient of Interaction

Fiber-fiber interactions are able to achieve expected interaction coefficient C_i values for several volume fraction and aspect ratio pairs with proper calibration. By varying the coefficient of friction, significant changes in the effective C_i are achieved. Fig. 6 shows a representative DEM simulation case for 11.58% by volume fiber filled simple shear flow with fibers emulating a 5.67 aspect ratio with a 0.67 coefficient of friction. The average alignment of the individual DEM fibers, DEM A_{ii}, agree well with the results from evaluating the Advani-Tucker equation (cf. equation 6) for the expected C_i from Eqn. 8. The A_{11} component shows that the initial transient and overshoot as well as the steady state values from Advani-Tucker are also present in DEM solution. The C_i value of 0.00407 computed through the optimization scheme agrees well with the curve predicted by Phan-Thien et al. [5] for this aspect ratio and volume fraction. The noise in the simulation data can be attributed to the number of fibers in the analysis region changing over time as the fibers are free to move in and out in the Z direction. Decreasing the domain volume by a factor of 8 exaggerates the noise as each fiber entering and leaving the analysis region is a larger percentage of the domain-averaged value. This effect is shown in Fig. 7 as both domain sizes have similar initial behavior and steady state values, but the larger domain has less variability at steady state. This effect continues with continually larger domains.

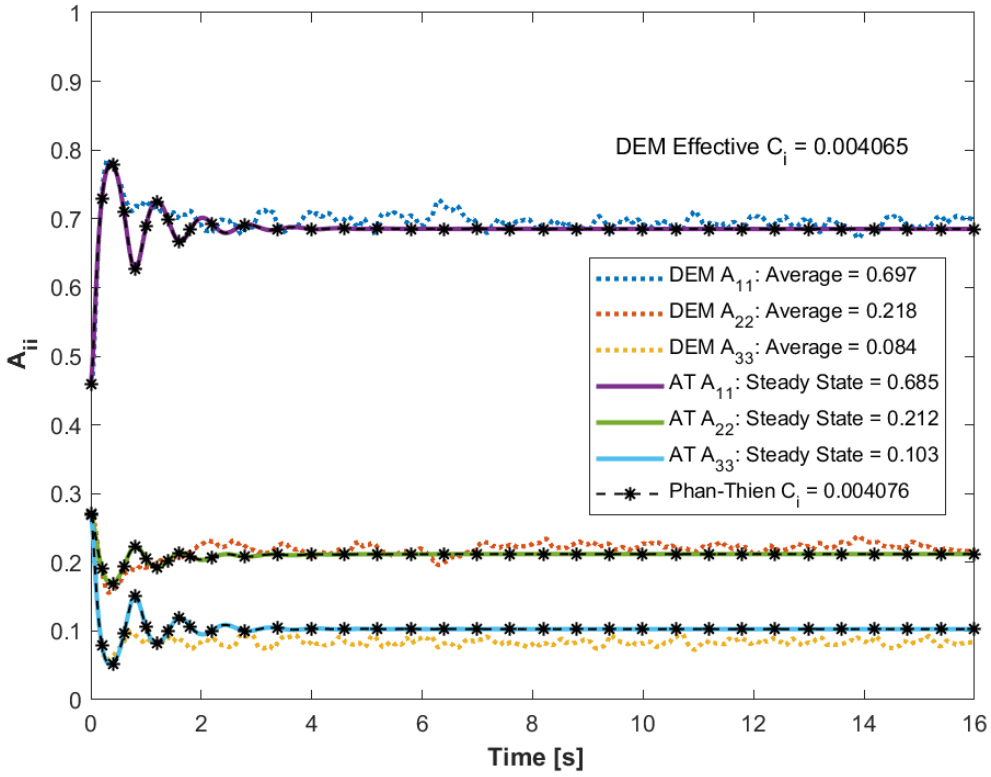

Fig. 6 - Fiber orientation tensor components with fitted Advani-Tucker solution plotted against the Advani-Tucker solution from expected Phan-Thien C_i value and DEM results

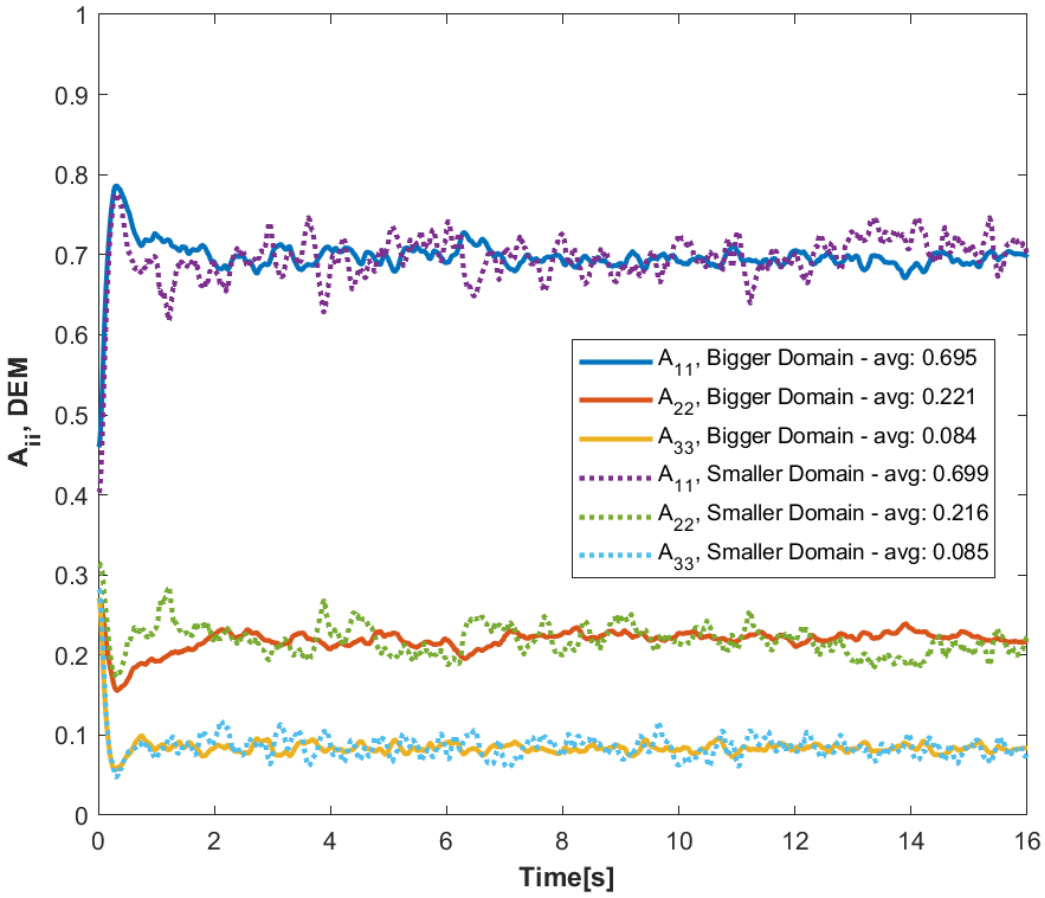

Fig. 7 - Average Orientation, A_{ii}, values for different domain sizes show increased domain size reduces noise and maintains steady-state values

The entire simulation domain for the smaller size domain with fibers colored by their individual p_1p_1 value is shown in Fig. 8 along with a histogram showing the distribution of p_1p_1 values for the initial, highest aligned, and final timesteps. The fibers started with randomly assigned position and orientation which quickly aligned before reaching a steady state with slightly less than the peak alignment. Notably, the highest alignment and steady state histograms vary primarily with a decrease in fibers with 0.95-1 p_1p_1 fibers that gets fairly evenly moved to the lower end of p_1p_1 values. With every fiber directly simulated, the orientation distribution is fully captured.

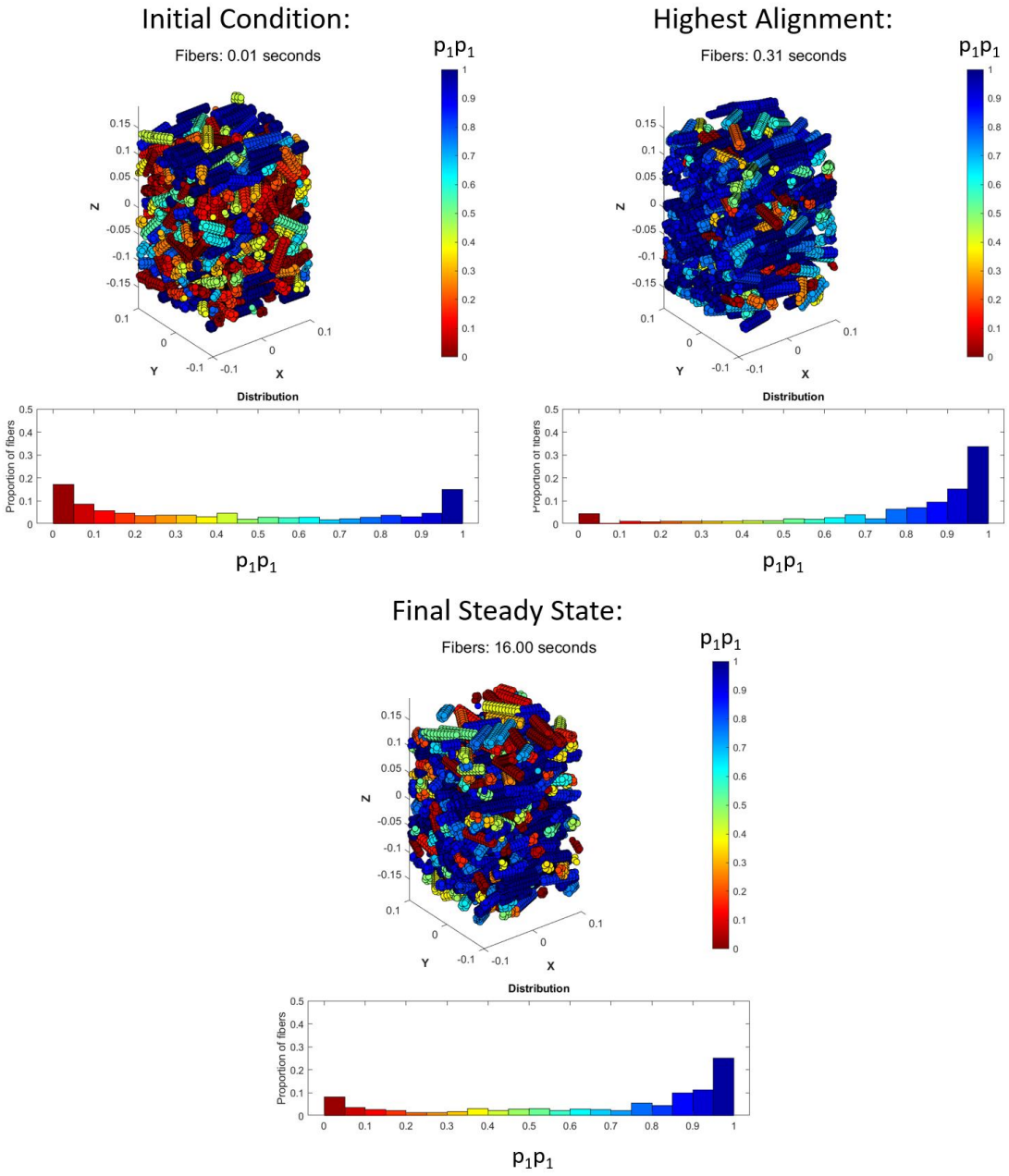

Fig. 8 - Fiber suspension simulation colored by individual fiber p_1p_1 with histograms of p_1p_1 distribution. Timesteps shown represent the initial condition, highest alignment, and final steady state conditions for the smaller domain.

These fiber suspension simulations have demonstrated repeatability in achieving the expected values for fiber orientation and C_i. Results from ten runs having identical properties other than newly seeded initial random position and orientation appear in Fig. 9. These results show that the averaged steady state simulation data consistently slightly underestimates A_{11} and A_{33} by approximately 0.01 compared to their fitted Advani-Tucker counterparts. The fitted effective C_i values obtained from these simulations are well centered around the expected value of 0.004 for the average volume fraction and aspect ratio pairs. Several other pairs have also been successfully calibrated as seen in Figure 10. These points are within the variability seen from other simulation

methods as well as physical experiments [5].The repeatability shown demonstrates that the contact models are effectively modeling fiber-fiber interaction to overcome any bias from initial conditions. The fiber suspension simulations maintain accuracy over other shear rates as well. The accuracy and repeatability of these calibrated fiber interactions lend confidence to the final application: additive manufacturing nozzles.

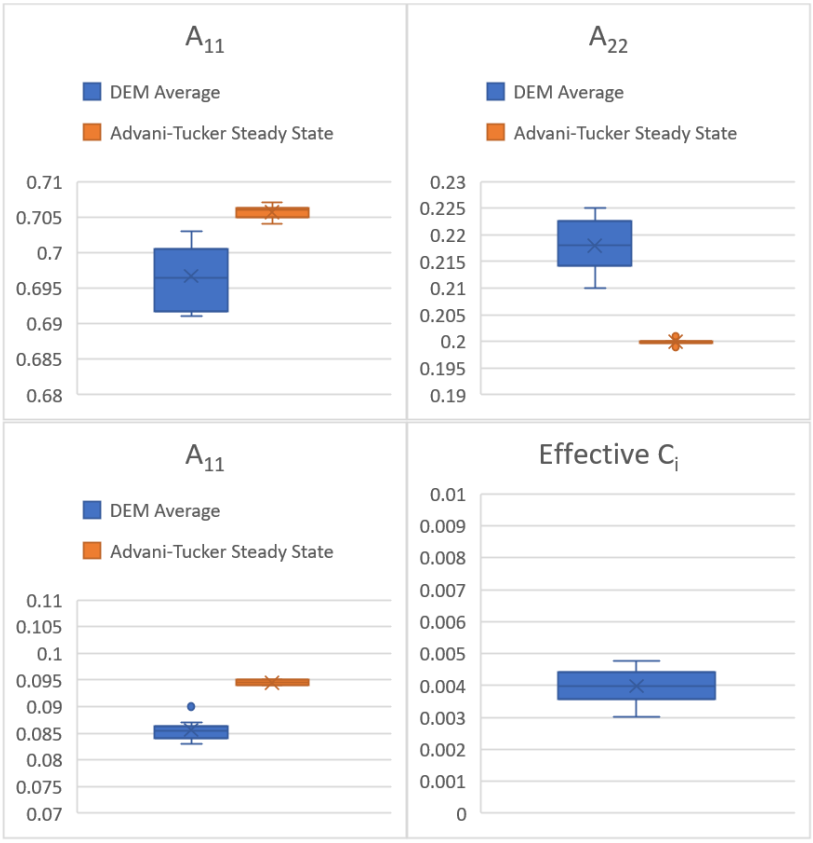

Fig. 9 - Box-whisker plots for 10 runs with shared parameters and uniquely randomized initial fiber position and orientation

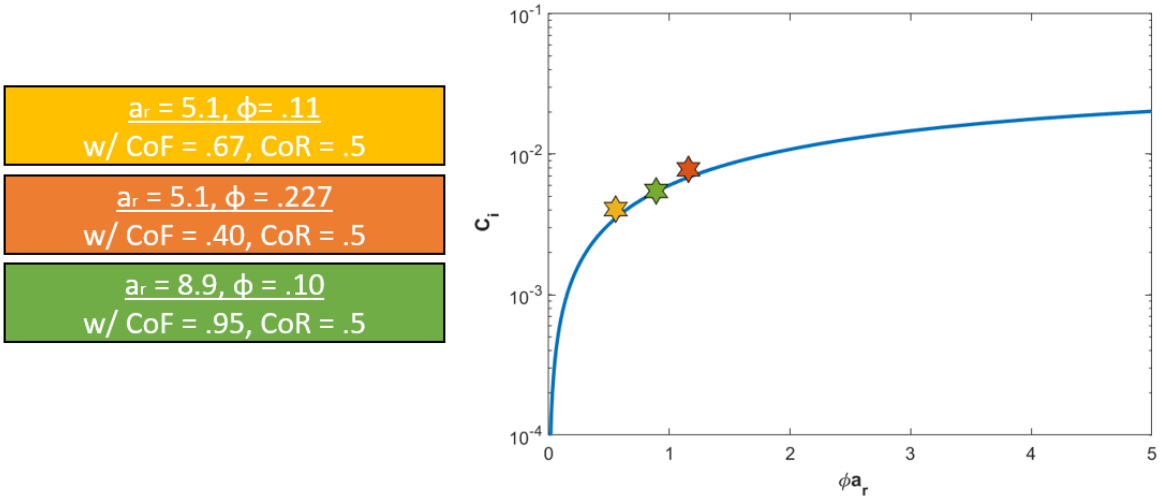

Fig. 10 - Calibrated volume fraction and aspect ratio pairs on the Phan-Thien Curve from Eqn. 7 for predicting C_i [5]

Small Scale Nozzle – Preliminary results

Small scale nozzle simulations provide enhanced insight into the fluid flow driven fiber dynamics that determine final part microstructure. With a well calibrated set of parameters from matching literature expectations for single and fiber suspension simulations, the small-scale nozzle simulations may additionally act as validation for more complex flows through comparison to experimental results. The nozzle CFD velocity magnitude field for the nozzle is shown in Figure 11. This field is imported into DEM along with the nozzle geometry for walls. Figure 12 shows the nozzle DEM simulations as the fibers enter the converged portion of the nozzle, fill the analysis region, and reach a steady state.

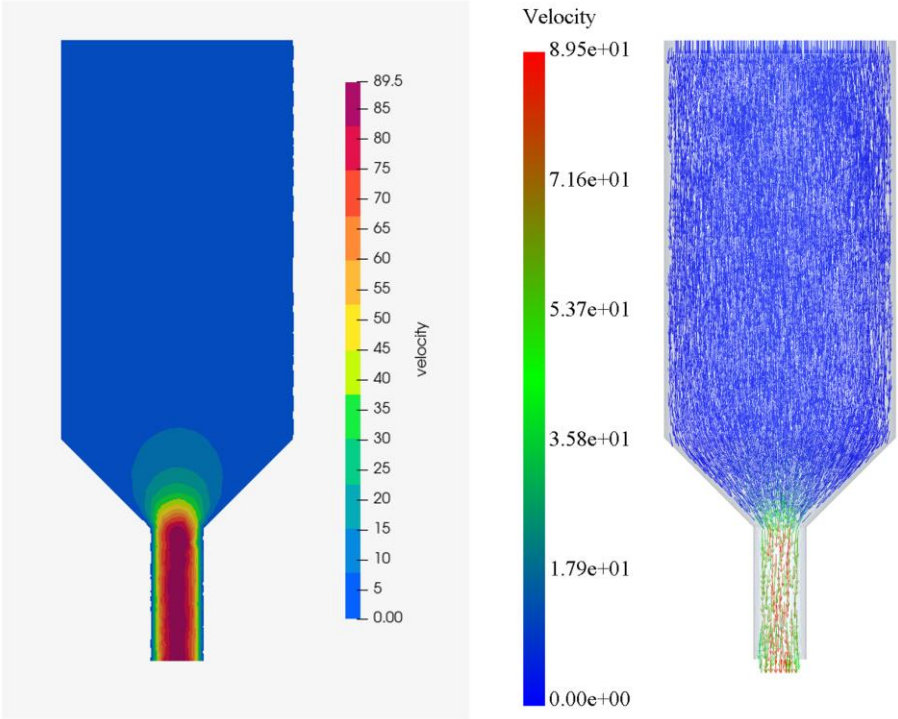

Fig. 11 – Contour plot of velocity magnitude on a cross section of the nozzle from the CFD solver (left) and the imported velocity vector field in DEM (right)

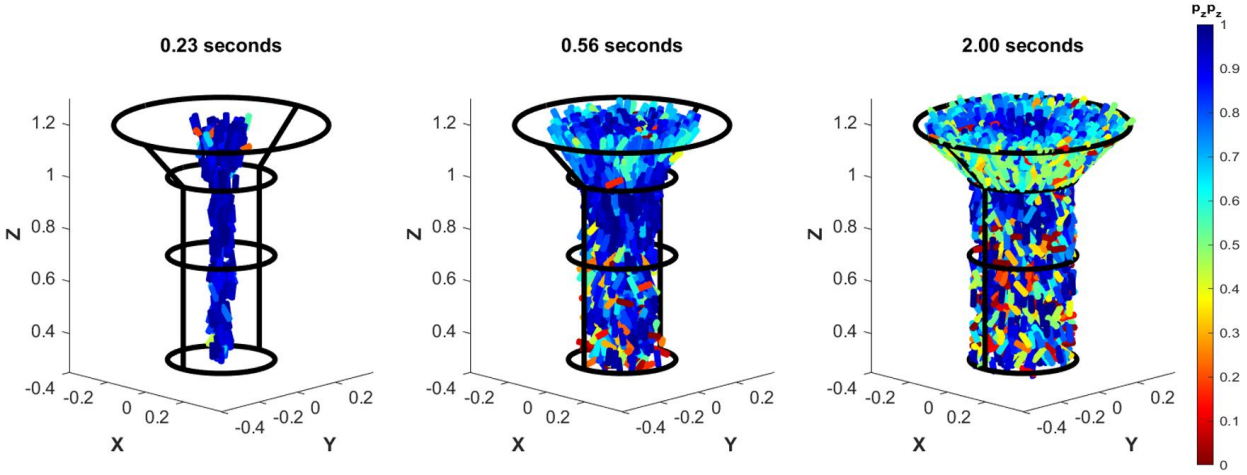

Fig. 12 – Fibers individually colored by their $p_z p_z$ value at different simulation times, showing the DEM fibers filling the nozzle and reaching steady state

The DEM simulation average fiber orientation tensor evolution over three regions of the flow domain is shown in Figure 13. The average steady state A_{11} value of 0.75 across the entire outlet of the nozzle aligns well with expectations from experimental nozzles extruding carbon fiber filled feedstocks [7,8]. The results for this case show a higher degree of alignment with the flow and higher volume fraction in the center of the analysis region. In contrast, the edges of the nozzle contain lower volume fraction and show a reduced fiber alignment. The slow flow with high shear and low volume fraction at the edges of the nozzles allows the low aspect ratio fibers to notably rotate out of alignment at the edges while the low shear and high volume fraction at the center prevents fibers from rotating away from their neighbors as they contact each other. This difference is possible since DEM does not assume a constant volume fraction, instead allowing fibers to evolve their spatial distribution as well as orientation. Longer fibers would potentially have more interaction with the walls of the nozzle and other fibers, preventing as much rotation away from alignment.

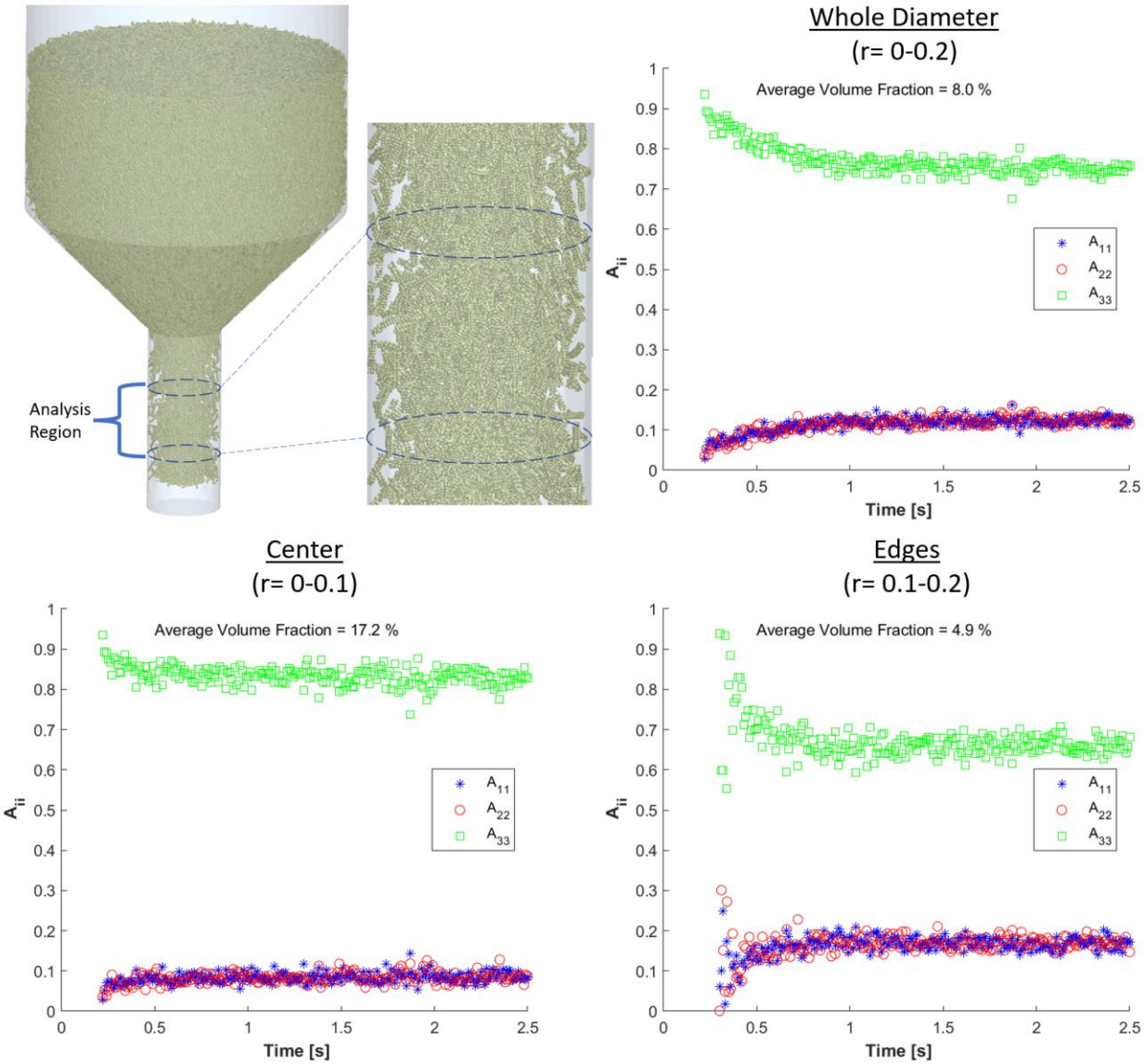

Fig. 13 – Fiber orientation and volume fraction in different regions of the converged portion of the nozzle

Data Availability

In DEM, every particle that makes up a fiber is effectively a sensor. Particles can report a wide variety of information for every fiber in every timestep simulated. Millions of particles are simultaneously directly simulated in a nozzle, creating a data rich environment. A few examples of this information are shown in Figure 14 for example nozzle cross sections. Factors can be easily analyzed over regions or on a fiber-by-fiber basis and compared against each other, such as how a fiber's deviation in alignment is impacted by number of contacts and the force of those contacts. The contact forces between the fibers and the walls can be used to model wear of nozzles.

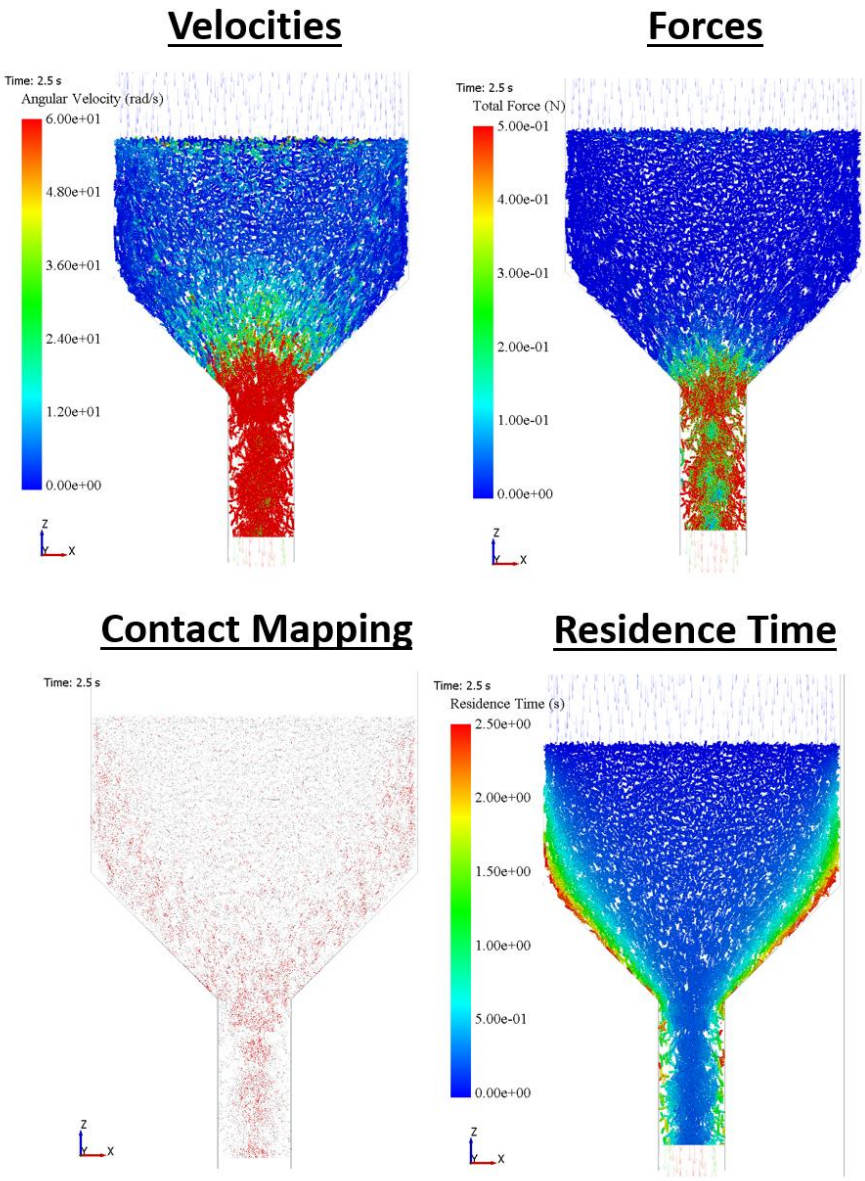

Fig. 14 – Example data available for each of the millions of particles simulated simultaneously

Conclusions

This paper presents a DEM/CFD approach for the flow of fiber suspension in a small scale polymer composite extrusion/deposition nozzle. Initial results show successful calibration of DEM fiber behavior in viscous simple shear flows. Single isolated fiber simulations show that the rotation of fibers in simple shear flow can be tuned through adjustment of the location of particles within the fiber's meta-particle layout to achieve Jeffery's orbit. Fiber suspension behavior is then calibrated by adjusting the particle coefficient of friction resulting in simulation results that are consistent with the well known Advani-Tucker orientation tensor method. These calibrated fibers are ultimately useful in creating high resolution, data rich simulations of fiber evolution in additive manufacturing nozzles. Future work on these simulations includes calibration in more complex flows, custom drag models, bidirectional DEM-CFD coupling, comparison of nozzle simulations to CT scans of nozzles, and calibration of fiber flexure and breakage.

References

[1] Jiang, D., and Smith, D. E., 2017, "Anisotropic Mechanical Properties of Oriented Carbon Fiber Filled Polymer Composites Produced with Fused Filament Fabrication," Additive Manufacturing, **18**, pp. 84–94.

[2] Brenken, B., Barocio, E., Favaloro, A., Kunc, V., and Pipes, R. B., 2018, "Fused Filament Fabrication of Fiber-Reinforced Polymers: A Review," Additive Manufacturing, **21**, pp. 1–16.

[3] Jeffery, G. B., and Filon, L. N. G., 1922, "The Motion of Ellipsoidal Particles Immersed in a Viscous Fluid," Proceedings of the Royal Society of London. Series A, Containing Papers of a Mathematical and Physical Character, **102**(715), pp. 161–179.

[4] Advani, S. G., and Tucker, C. L., 1987, "The Use of Tensors to Describe and Predict Fiber Orientation in Short Fiber Composites," Journal of Rheology, **31**(8), pp. 751–784.

[5] Phan-Thien, N., Fan, X.-J., Tanner, R. I., and Zheng, R., 2002, "Folgar–Tucker Constant for a Fibre Suspension in a Newtonian Fluid," Journal of Non-Newtonian Fluid Mechanics, **103**(2), pp. 251–260.

[6] Kugler, S. K., Kech, A., Cruz, C., and Osswald, T., 2020, "Fiber Orientation Predictions—A Review of Existing Models," Journal of Composites Science, **4**(2), p. 69.

[7] Heller, B. P., Smith, D. E., and Jack, D. A., 2019, "Planar Deposition Flow Modeling of Fiber Filled Composites in Large Area Additive Manufacturing," Additive Manufacturing, **25**, pp. 227–238.

[8] Heller, B. P., Smith, D. E., and Jack, D. A., 2016, "Effects of Extrudate Swell and Nozzle Geometry on Fiber Orientation in Fused Filament Fabrication Nozzle Flow," Additive Manufacturing, **12**, pp. 252–264.

[9] Zhang, D., E. Smith, D., A. Jack, D., and Montgomery-Smith, S., 2011, "Numerical Evaluation of Single Fiber Motion for Short-Fiber-Reinforced Composite Materials Processing," Journal of Manufacturing Science and Engineering, **133**(051002).

[10] Zhang, D., and Smith, D., 2015, "Finite Element Based Brownian Dynamics Simulation of Nanofiber Suspensions Using Monte-Carlo Method," Journal of Micro and Nano-Manufacturing, **3**.

[11] Awenlimobor, A., Wang, Z., and Smith, D. E., 2021, "Physical Modeling: Simulation of Micro-Void Development within Large Scale Polymer Composite Deposition Beads," University of Texas at Austin.

[12] Lewicki, J. P., Rodriguez, J. N., Zhu, C., Worsley, M. A., Wu, A. S., Kanarska, Y., Horn, J. D., Duoss, E. B., Ortega, J. M., Elmer, W., Hensleigh, R., Fellini, R. A., and King, M. J., 2017, "3D-Printing of Meso-Structurally Ordered Carbon Fiber/Polymer Composites with Unprecedented Orthotropic Physical Properties," Sci Rep, **7**(1), p. 43401.

[13] Yashiro, S., Sasaki, H., and Sakaida, Y., 2012, "Particle Simulation for Predicting Fiber Motion in Injection Molding of Short-Fiber-Reinforced Composites," Composites Part A: Applied Science and Manufacturing, **43**(10), pp. 1754–1764.

[14] Inoue, A., Morita, K., Tanaka, T., Arao, Y., and Sawada, Y., 2013, "Effect of Screw Design on Fiber Breakage and Dispersion in Injection-Molded Long Glass-Fiber-Reinforced Polypropylene," Journal of Composite Materials, **49**, pp. 75–84.

[15] Cundall, P. A., and Strack, O. D. L., 1979, "A Discrete Numerical Model for Granular Assemblies," Géotechnique, **29**(1), pp. 47–65.

[16] Kafui, K. D., Thornton, C., and Adams, M. J., 2002, "Discrete Particle-Continuum Fluid Modelling of Gas–Solid Fluidised Beds," Chemical Engineering Science, **57**(13), pp. 2395–2410.
[17] Potyondy, D. O., and Cundall, P. A., 2004, "A Bonded-Particle Model for Rock," International Journal of Rock Mechanics and Mining Sciences, **41**(8), pp. 1329–1364.
[18] Sayah, N., and Smith, D. E., 2022, "Effect of Process Parameters on Void Distribution, Volume Fraction, and Sphericity within the Bead Microstructure of Large-Area Additive Manufacturing Polymer Composites," Polymers, **14**(23), p. 5107.
[19] Schiller, L., and Naumann, A., 1933, "A Drag Coefficient Correlation," Vdi Zeitung, pp. 318–320.
[20] Zhou, Y. C., Wright, B. D., Yang, R. Y., Xu, B. H., and Yu, A. B., 1999, "Rolling Friction in the Dynamic Simulation of Sandpile Formation," Physica A: Statistical Mechanics and its Applications, **269**(2), pp. 536–553.
[21] Ai, J., Chen, J.-F., Rotter, J. M., and Ooi, J. Y., 2011, "Assessment of Rolling Resistance Models in Discrete Element Simulations," Powder Technology, **206**(3), pp. 269–282.